nature photonics

LETTERS

PUBLISHED ONLINE: 20 JULY 2015 | DOI: 10.1038/NPHOTON.2015.123

Observation of a Luttinger-liquid plasmon in metallic single-walled carbon nanotubes

Zhiwen Shi[1*†], Xiaoping Hong[1†], Hans A. Bechtel[2], Bo Zeng[1], Michael C. Martin[2], Kenji Watanabe[3], Takashi Taniguchi[3], Yuen-Ron Shen[1,4] and Feng Wang[1,4,5*]

Surface plasmons[1], collective oscillations of conduction electrons, hold great promise for the nanoscale integration of photonics and electronics[1–4]. However, nanophotonic circuits based on plasmons have been significantly hampered by the difficulty in achieving broadband plasmonic waveguides that simultaneously exhibit strong spatial confinement, a high quality factor and low dispersion. Quantum plasmons, where the quantum mechanical effects of electrons play a dominant role, such as plasmons in very small metal nanoparticles[5,6] and plasmons affected by tunnelling effects[7], can lead to novel plasmonic phenomena in nanostructures. Here, we show that a Luttinger liquid[8,9] of one-dimensional Dirac electrons in carbon nanotubes[10–13] exhibits quantum plasmons that behave qualitatively differently from classical plasmon excitations. The Luttinger-liquid plasmons propagate at 'quantized' velocities that are independent of carrier concentration or excitation wavelength, and simultaneously exhibit extraordinary spatial confinement and high quality factor. Such Luttinger-liquid plasmons could enable novel low-loss plasmonic circuits for the subwavelength manipulation of light.

Quantum-confined electrons in one dimension behave as a Luttinger liquid, a strongly correlated electronic matter distinctly different from the quasi-free electrons described by the Fermi liquid[8,9]. A defining characteristic of the Luttinger liquid is the spin-charge separation, where the spin and charge excitations propagate at different speeds. The elementary charge excitations of the Luttinger liquid are one-dimensional quantum plasmons, which differ substantially from their classical counterparts. Classically, plasmons are determined by the free electron density and effective mass, as in Drude conductivity, but this description completely breaks down for Luttinger-liquid plasmons, which are instead determined by the electron Fermi velocity and the number of quantum conducting channels[10,11]. Metallic single-walled carbon nanotubes (SWNTs), with their extraordinary one-dimensional quantum confinement, provide the ideal platform to explore such Luttinger-liquid plasmons. Due to this strong quantum confinement, Luttinger-liquid plasmons in SWNTs with a diameter of 1 nm should persist to visible frequencies before the first intersubband transition appears[14]. In addition, the forbidden backscattering of Dirac electrons[15,16], evidenced by ballistic transport up to micrometre lengths[17–19] in metallic SWNTs, can lead to strongly confined but low-loss Luttinger-liquid plasmons. The experimental observation of such Luttinger-liquid plasmons in SWNTs has remained an outstanding challenge for over a decade, although previous electrical transport and photoemission measurements have shown the presence of Luttinger liquid in SWNTs[12,13,20].

Here, we report the first observation of Luttinger-liquid plasmons in SWNTs using infrared scattering-type scanning near-field optical microscopy (s-SNOM)[21–23]. We show that the Luttinger-liquid plasmons can be excited in a broad frequency range and that they propagate at a 'quantized' velocity in individual SWNTs. This velocity, unlike classical plasmon oscillations, does not depend on the free carrier density and varies only weakly with the plasmon frequency or nanotube diameter. Instead, it is mainly determined by the quantized number of conducting channels in SWNTs. At the same time, Luttinger-liquid plasmons in SWNTs simultaneously exhibit strong spatial confinement and a high-quality factor, a most sought-after feature in plasmonics[24]. Our observed quantum plasmon behaviour agrees quantitatively with the Luttinger-liquid theory of nanotubes. Such Luttinger-liquid plasmons in SWNTs hold great potential for novel broadband plasmonic waveguides and nanophotonic circuits with low dispersion, high quality factor and strong subwavelength confinement.

Metallic SWNTs with diameters ranging from 1.2 nm to 1.7 nm were grown by the arc-discharge method, and were then suspended in a micelle solution using ultrasonication, and purified to 95% metallic SWNTs using density gradient ultracentrifugation[25]. The nanotube solution was then spin-coated onto thin hexagonal boron nitride (hBN) flakes on SiO_2/Si substrates to yield isolated individual and small bundles of SWNTs. hBN was chosen as a substrate because it is atomically flat and extremely clean, which facilitates the observation of Luttinger-liquid plasmons in the nanotubes. In contrast, it is very difficult to observe plasmon excitation in nanotubes spin-coated directly on SiO_2/Si substrates. Plasmons in these metallic SWNTs were probed using infrared s-SNOM, as shown in Fig. 1a. Infrared light at 6.1 μm or 10.6 μm was focused onto the apex of a metal-coated atomic force microscope (AFM) tip with a radius of curvature of $r \approx 25$ nm, the large near-field momentum of which enabled optical excitation of plasmons in the SWNTs. The excited plasmon wave propagated along the SWNT and was reflected at the nanotube end. The back-reflected plasmon wave interfered with the excitation wave under the tip, which modified the intensity of the tip-scattered infrared radiation measured by an HgCdTe detector in the far field. As the tip was scanned along the nanotube, the scattered infrared radiation varied periodically, with intensity peaks appearing at positions of constructive interference[23,26,27]. Figure 1b presents a representative infrared s-SNOM image of a metallic SWNT, the topography of which was recorded simultaneously (shown in the inset). Prominent plasmon oscillation

[1]Department of Physics, University of California at Berkeley, Berkeley, California 94720, USA. [2]Advanced Light Source Division, Lawrence Berkeley National Laboratory, Berkeley, California 94720, USA. [3]Advanced Materials Laboratory, National Institute for Materials Science, 1-1 Namiki, Tsukuba 305-0044, Japan. [4]Materials Science Division, Lawrence Berkeley National Laboratory, Berkeley, California 94720, USA. [5]Kavli Energy NanoSciences Institute at the University of California, Berkeley and the Lawrence Berkeley National Laboratory, Berkeley, California 94720, USA. †These authors contributed equally to this work. *e-mail: fengwang76@berkeley.edu; zhiwen22@gmail.com

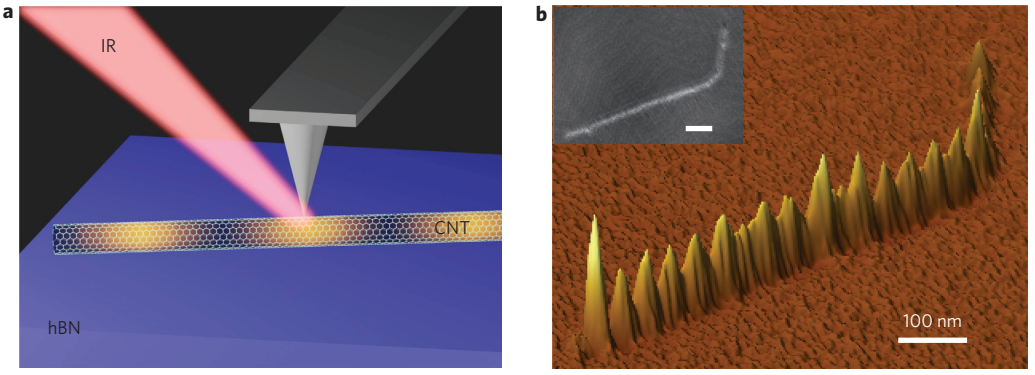

Figure 1 | Infrared s-SNOM of one-dimensional plasmons in carbon nanotubes. a, Illustration of s-SNOM. Infrared (IR) light is focused onto the apex of a metal-coated AFM tip, the large near-field momentum of which enables optical excitation of plasmons in the carbon nanotube (CNT) on a hBN substrate. Interference between the tip-excited plasmon wave and its reflection from the nanotube end leads to periodic modulation of tip-scattered infrared radiation measured by an HgCdTe detector in the far field. **b**, Three-dimensional plot of the near-field scattering intensity (height) along a representative SWNT. Prominent modulation of the infrared scattering intensity from the one-dimensional plasmon can be observed over the whole nanotube. Inset: AFM topography image of the same SWNT. Scale bars, 100 nm.

along the entire length of the nanotube can be clearly observed under ambient conditions.

We systematically investigated plasmons in different SWNTs on hBN substrates. The nanotubes spin-coated on hBN were first characterized by the recently developed *in situ* single tube spectroscopy[28]. Figure 2a,b presents optical spectra of two representative individual SWNTs, which are characterized by one or two prominent optical resonances. From these resonances we can identify the nanotube chirality to be (11,11) and (15,6)[14], corresponding to metallic nanotubes with diameters of 1.49 nm and 1.47 nm, respectively. Figure 2c presents the optical spectrum of a typical small bundle, which is characterized by broader optical features

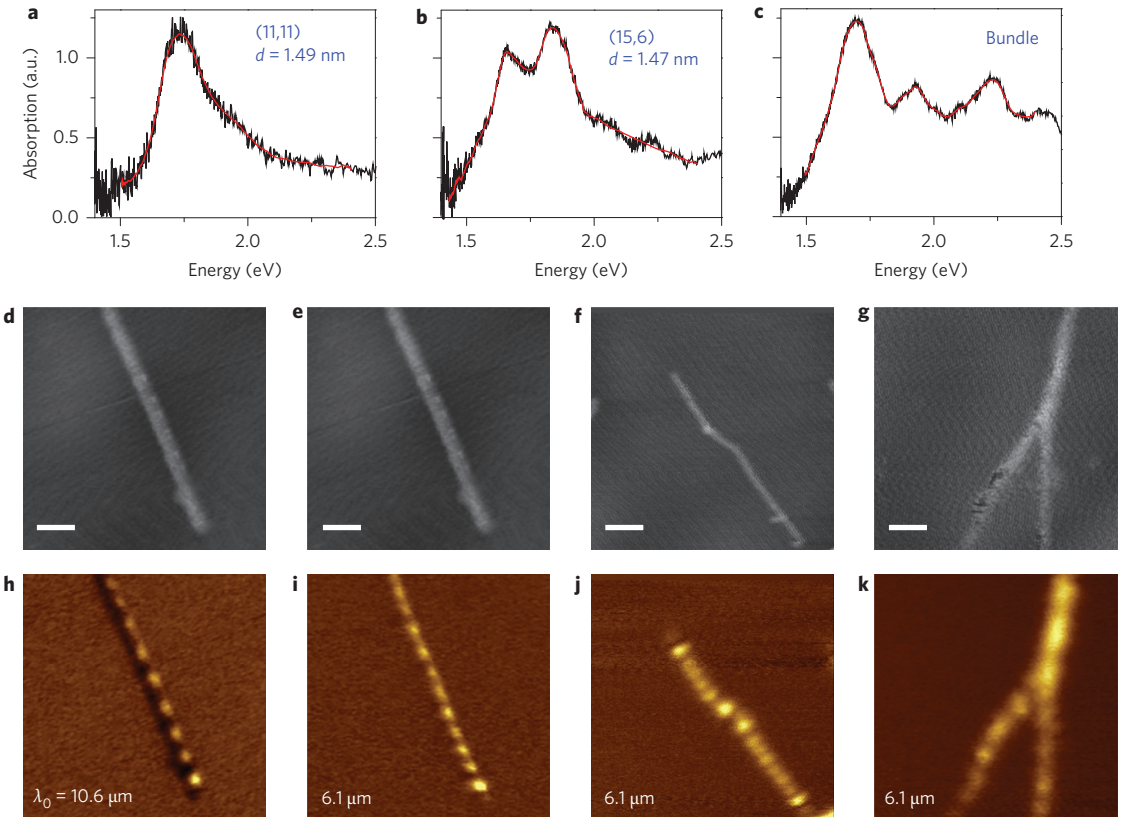

Figure 2 | Luttinger-liquid plasmons in carbon nanotubes. a–c, Optical spectra (black) of individual metallic SWNTs with chiralities of (11,11) (**a**) and (15,6) (**b**) and of a small nanotube bundle (**c**). Red curves are guiding lines. **d–g**, AFM topography images of representative nanotube samples. **h–k**, Infrared s-SNOM images for different excitation wavelengths for the tubes shown in **d–g**. **h**,**i**, Near-field infrared images for the same nanotube with 10.6 μm (**h**) and 6.1 μm (**i**) excitation. The infrared scattering oscillation period is consistent with a linear scaling behaviour with excitation wavelength. **i–k**, Infrared scattering oscillation in different nanotubes with 6.1 μm excitation. In **k**, in particular, the oscillation period is seen to become longer when tubes coalesce into bigger bundles. Scale bars, 100 nm.

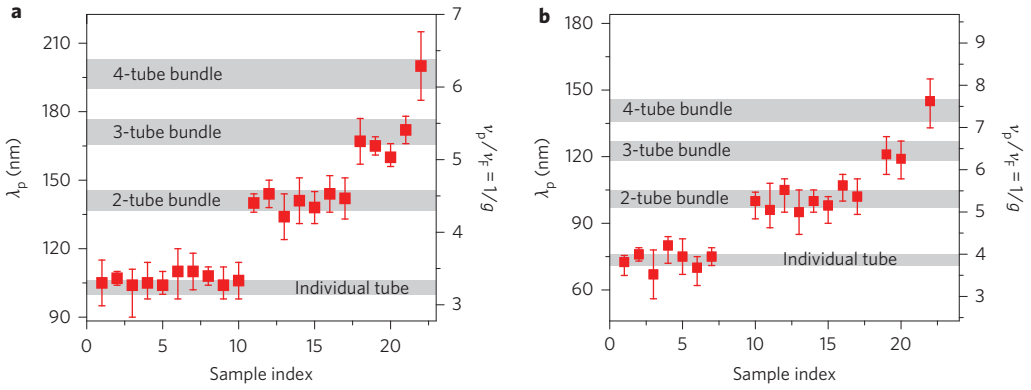

Figure 3 | Quantized Luttinger-liquid plasmon propagation velocity. a,b, The plasmon wavelength, λ_p (left axis), and propagation velocity, v_p/v_F (or $1/g$, right axis), for different nanotubes with 10.6 μm (**a**) and 6.1 μm (**b**) excitation. The Luttinger-liquid plasmon shows quantization propagation velocities around a few discrete values, which can be approximated by the simple ratio $1{:}\sqrt{2}{:}\sqrt{3}{:}\sqrt{4}$, related to the quantized number of conducting channels in different nanotubes. The experimental data agree well with Luttinger-liquid theory (shaded ribbons), where we have included the effects of a finite SWNT diameter distribution (1.2–1.7 nm) and effective dielectric constants of 2.1 for 10.6 μm and 1.0 for 6.1 μm from substrate screening. Error bars represent the uncertainty from fitting the one-dimensional plasmon profiles.

and more resonances. We found that the spin-coated nanotubes are either individual SWNTs or small bundles, and almost all individual SWNTs are metallic, consistent with the high metallic nanotube percentage in these samples.

Figure 2d–g shows four AFM topography images of SWNTs on hBN substrates, and Fig. 2h–k presents the corresponding near-field infrared s-SNOM images of one-dimensional plasmons in these nanotubes with 10.6 μm or 6.1 μm photon excitation. Periodic oscillation of the tip-induced infrared scattering from one-dimensional Luttinger-liquid plasmons is apparent in all nanotubes. However, the oscillation period varies for different infrared excitation wavelengths and in different nanotubes. Figure 2h,i shows near-field infrared scattering images with 10.6 μm and 6.1 μm excitation, respectively, for the same nanotube. The oscillation period is longer with 10.6 μm excitation, and the oscillation period and excitation wavelength have almost the same ratio, consistent with a linear scaling. Figure 2i–k display near-field infrared scattering images in different nanotubes. Figure 2k clearly shows that the oscillation period becomes longer in a bundle than in the constituent nanotubes.

We next determined the Luttinger-liquid plasmon wavelength and propagation velocity in different nanotube samples. The scattering peaks in the infrared s-SNOM images (Fig. 2h–k) are determined by constructive interference where the reflected plasmon accumulates a phase change $\Delta\phi = 2 \times 2\pi L/\lambda_p + \phi_0 = 2m\pi$. Here, L is the distance between the tip and tube end, λ_p is the plasmon wavelength, ϕ_0 is the reflection phase change, and m is an integer. The plasmon wavelength λ_p is therefore simply twice the oscillation period observed in the infrared s-SNOM images. The propagation velocity of a one-dimensional plasmon (v_p) can be readily calculated from its frequency and wavelength by $v_p = \nu \times \lambda_p = c \times \lambda_p/\lambda_0$, where ν is the frequency, c is the speed of light, and λ_0 is the free-space photon wavelength.

Figure 3a,b plots the plasmon wavelength (λ_p, left axis) and the corresponding plasmon velocity (v_p/v_F, right axis) in different nanotubes with 10.6 μm and 6.1 μm excitation, respectively. We found that the plasmon velocity exhibits a quantized behaviour. Of 22 measured nanotubes with 10.6 μm excitation, ten tubes had a plasmon velocity quantized at a minimum value of $3.2v_F$, another seven nanotubes had v_p clustered around $4.4v_F$ and the others had v_p values of $5.3v_F$ and $6.2v_F$. These quantized velocities can be well approximated by the simple ratio $1{:}\sqrt{2}{:}\sqrt{3}{:}\sqrt{4}$. Similar quantized velocities are also observed for 6.1 μm excitation, although the absolute values are slightly larger. Such quantized plasmon propagation velocities in as-prepared nanotubes, which have different diameters and carrier concentrations from environmental doping, differ qualitatively from the behaviour of classical plasmons.

To understand the unusual propagation of Luttinger-liquid plasmons, we quantitatively examined Luttinger-liquid behaviour in individual and small bundles of metallic SWNTs. Pioneering work by Kane and colleagues shows that interacting electrons in metallic SWNTs are described by strongly renormalized Luttinger liquid[10]. This Luttinger liquid in SWNTs is fully characterized by the Luttinger-liquid parameter g, which describes the type and strength of the interaction. Non-interacting electron gases are described by $g = 1$, while attractive interactions have $g > 1$ and repulsive interactions have $g < 1$. The plasmon velocity v_p is related to g simply by $v_p = v_F/g$. For individual suspended SWNTs of radius R screened by a concentric metal shell of radius R_s, the Luttinger-liquid parameter can be calculated quantitatively as $1/g = \sqrt{1 + (8e^2/\pi\hbar v_F)\ln(R_s/R)}$, where the second term arises from long-range Coulomb interactions and is proportional to the number of conducting channels and the unit length capacitance between the coaxial nanotube and metal shell[10]. For plasmons in small nanotube bundles residing on a substrate, the Coulomb interaction term is modified, and the Luttinger-liquid parameter becomes

$$\frac{1}{g} = \frac{v_p}{v_F} \approx \sqrt{1 + \left(\frac{2 \times 4Ne^2}{\varepsilon_{eff}\pi\hbar v_F}\right)\ln\left(\frac{\lambda_p}{2\pi R_t}\right)} \quad (1)$$

where N is the number of SWNTs in a bundle and $4N$ is the number of quantized conducting channels, ε_{eff} is the effective dielectric constant due to substrate screening, R_t is the effective radius of the nanotube bundle, and the plasmon wavelength λ_p determines the cutoff length of Coulomb interactions (see Supplementary Sections 2 and 3 for details).

Luttinger-liquid theory indeed predicts very unusual plasmon propagation velocities. Unlike classical plasmon excitations, the Luttinger-liquid plasmon velocity in equation (1) does not depend on the electron density at all. Instead, it is mainly determined by the quantized number of conducting channels $4N$. The plasmon velocity varies with R_t and λ_p only weakly in a logarithmic fashion. The theory accounts for our observed quantization of the plasmon propagation speed, where plasmons travel at velocities with a ratio of around $1{:}\sqrt{2}{:}\sqrt{3}{:}\sqrt{4}$ for individual SWNTs and bundles containing two, three and four tubes, and nanotubes with different

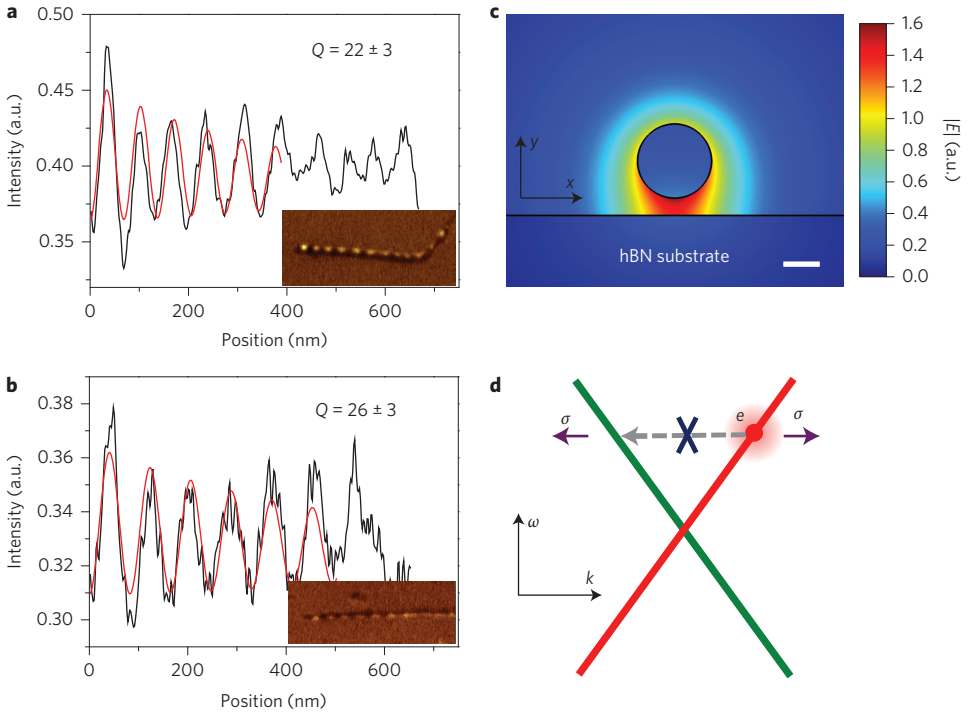

Figure 4 | Long-range quantum plasmons in nanotubes. a,**b**, Oscillation of near-field infrared scattering intensity from one-dimensional plasmons in two metallic nanotubes. Fitting (red lines) of the oscillation near the nanotube end yields a plasmon quality factor, Q, of over 20 in both SWNTs, although the plasmon wavelength, λ_p, is only ~1/100 of the free-space wavelength, λ_0. **c**, Numerical simulation of the electrical field distribution of the one-dimensional plasmon around a nanotube with a diameter of 2 nm, which shows transverse confinement of the electrical field within a few nanometres, less than 1/1,000 of λ_0. Scale bar, 1 nm. **d**, Illustration of the chirality of Dirac electrons in SWNTs, where left- and right-moving electrons are characterized by opposite pseudo-spins. Backscattering is forbidden for such Dirac electrons, and it leads to the remarkably low loss of one-dimensional nanotube plasmons, even with strong spatial confinement.

diameters and carrier densities have almost the same plasmon velocity. More quantitatively, we calculated the predicted range of plasmon velocities for N-tube bundles using equation (1). These are shown as shaded areas in Fig. 3. We included a tube diameter distribution from 1.2 nm to 1.7 nm, approximated the effective radius of a nanotube bundle as $\sqrt{N}R$, and used effective dielectric constants of $\varepsilon_{eff} = 2.1$ at 10.6 μm and $\varepsilon_{eff} = 1.0$ at 6.1 μm due to dielectric screening from the hBN substrates (see Supplementary Sections 2 and 3 for more details). This Luttinger-liquid theory, which is free of adjustable parameters, quantitatively matches the experimental data. Note that, although the plasmon frequency at 6.1 μm is almost twice that at 10.6 μm, the plasmon velocity changes by only 15%, largely due to the frequency-dependent hBN dielectric constant. This highlights the low dispersion of Luttinger-liquid plasmons in SWNTs.

Luttinger-liquid plasmons in metallic SWNTs also exhibit a remarkable combination of strong spatial confinement and high quality factors, two key figures of merit for plasmonics[24]. The Luttinger-liquid plasmons are characterized by extraordinary sub-wavelength confinement. The plasmon wavelength along the nanotube is as small as 1/100 of the free-space light wavelength (Fig. 3 and insets of Fig. 4a,b). The transverse confinement is even stronger. Figure 4c shows the numerically simulated transverse electric field distribution of a one-dimensional plasmon in a SWNT, which shows a spatial confinement of ~1 nm, less than 1/1,000 of $\lambda_0 = 10.6$ μm. Strikingly, such a strongly confined one-dimensional plasmon can propagate over a long distance with little attenuation in SWNTs. Figure 4a,b presents the oscillating infrared scattering intensity along two different nanotubes (black lines). We can estimate the quality factor Q of the corresponding one-dimensional plasmon by fitting the oscillation with an exponential decay of the form $e^{-2\pi x/(Q\cdot\lambda_p)}\sin((4\pi x)/\lambda_p)$ from the nanotube end (red line in Fig. 4a,b). Although fitting over the whole nanotube is difficult due to fluctuations in the near-field infrared scattering intensity, good agreement can be obtained for clean oscillations near the end of a nanotube, yielding a quality factor of over 20 in the SWNTs shown in Fig. 4a,b. This combination of extraordinary spatial confinement (λ_p/λ_0 of ~1/100) and high quality factor ($Q > 20$) in nanotube plasmons is unprecedented. Typically, strong spatial confinement of a plasmon can only be achieved at the expense of a low quality factor due to the absorption loss of metals. For instance, a two-dimensional surface plasmon at a silver/air interface has a quality factor of ~16 with $\lambda_p/\lambda_0 = 1.16$ at 400 nm, but Q worsens to ~2.27 when λ_p/λ_0 increases to 1.51 at 350 nm (ref. 29). Similarly, two-dimensional plasmons in graphene can have rather good spatial confinement (λ_p/λ_0 of ~1/50), but the quality factor Q is limited to ~5 (refs 26 and 27).

The remarkably low loss of Luttinger-liquid plasmons in SWNTs presumably originates from the unique properties of one-dimensional chiral electrons in carbon nanotubes. Electrons in metallic SWNTs are described by relativistic Dirac fermions, where forward- and backward-moving electrons have opposite chiral handedness. Such chiral electrons cannot be backscattered by slowly varying the charge impurity potential or acoustic phonons, because the electron handedness has to be preserved (Fig. 4d)[15,16,30]. The protection from backscattering eliminates all loss channels in one-dimensional SWNTs. This contrasts with two-dimensional graphene, where Dirac electrons can still be scattered to angles different from 180° even with forbidden backscattering. The lack of electron backscattering in SWNTs leads to a very long electron mean free path in electrical transport, even for nanotubes on SiO_2/Si substrates at room temperature[18,19]. Here, it gives

rise to Luttinger-liquid plasmons with low absorption loss and long-range propagation, although the spatial confinement is strongly subwavelength.

Our direct observation of Luttinger-liquid plasmons opens up exciting new opportunities to explore both one-dimensional Luttinger-liquid physics and quantum plasmons in carbon nanotubes, the properties of which can be manipulated through electrostatic gating, mechanical strain and external magnetic field. Although our studies have focused on Luttinger-liquid plasmons at infrared wavelengths, the Luttinger-liquid behaviour in SWNTs should be valid over a broad frequency range up to visible frequencies because the first intersubband transition is above 1.7 eV for metallic nanotubes of 1.5 nm diameter (Fig. 2a,b) due to strong quantum confinement in the SWNTs[14]. The combination of low dispersion, high quality factor and strong subwavelength confinement in Luttinger-liquid plasmon holds great potential for novel plasmonic and nanophotonic devices over a broad frequency range, including telecom wavelengths.

Received 11 March 2015; accepted 15 June 2015;
published online 20 July 2015

References

1. Barnes, W. L., Dereux, A. & Ebbesen, T. W. Surface plasmon subwavelength optics. *Nature* **424,** 824–830 (2003).
2. Gramotnev, D. K. & Bozhevolnyi, S. I. Plasmonics beyond the diffraction limit. *Nature Photon.* **4,** 83–91 (2010).
3. Schuller, J. A. *et al.* Plasmonics for extreme light concentration and manipulation. *Nature Mater.* **9,** 193–204 (2010).
4. Pendry, J. B., Aubry, A., Smith, D. R. & Maier, S. A. Transformation optics and subwavelength control of light. *Science* **337,** 549–552 (2012).
5. Halperin, W. P. Quantum size effects in metal particles. *Rev. Mod. Phys.* **58,** 533–606 (1986).
6. Scholl, J. A., Koh, A. L. & Dionne, J. A. Quantum plasmon resonances of individual metallic nanoparticles. *Nature* **483,** 421–427 (2012).
7. Tan, S. F. *et al.* Quantum plasmon resonances controlled by molecular tunnel junctions. *Science* **343,** 1496–1499 (2014).
8. Luttinger, J. M. An exactly soluble model of a many-fermion system. *J. Math. Phys.* **4,** 1154–1162 (1963).
9. Voit, J. One-dimensional Fermi liquids. *Rep. Prog. Phys.* **58,** 977–1116 (1995).
10. Kane, C., Balents, L. & Fisher, M. P. A. Coulomb interactions and mesoscopic effects in carbon nanotubes. *Phys. Rev. Lett.* **79,** 5086–5089 (1997).
11. Egger, R. & Gogolin, A. O. Effective low-energy theory for correlated carbon nanotubes. *Phys. Rev. Lett.* **79,** 5082–5085 (1997).
12. Bockrath, M. *et al.* Luttinger-liquid behaviour in carbon nanotubes. *Nature* **397,** 598–601 (1999).
13. Yao, Z., Postma, H. W. C., Balents, L. & Dekker, C. Carbon nanotube intramolecular junctions. *Nature* **402,** 273–276 (1999).
14. Liu, K. *et al.* An atlas of carbon nanotube optical transitions. *Nature Nanotech.* **7,** 325–329 (2012).
15. Ando, T., Nakanishi, T. & Saito, R. Berry's phase and absence of back scattering in carbon nanotubes. *J. Phys. Soc. Jpn* **67,** 2857–2862 (1998).
16. McEuen, P. L., Bockrath, M., Cobden, D. H., Yoon, Y. G. & Louie, S. G. Disorder, pseudospins, and backscattering in carbon nanotubes. *Phys. Rev. Lett.* **83,** 5098–5101 (1999).
17. Javey, A., Guo, J., Wang, Q., Lundstrom, M. & Dai, H. J. Ballistic carbon nanotube field-effect transistors. *Nature* **424,** 654–657 (2003).
18. Park, J. Y. *et al.* Electron–phonon scattering in metallic single-walled carbon nanotubes. *Nano Lett.* **4,** 517–520 (2004).
19. Purewal, M. S. *et al.* Scaling of resistance and electron mean free path of single-walled carbon nanotubes. *Phys. Rev. Lett.* **98,** 186808 (2007).
20. Ishii, H. *et al.* Direct observation of Tomonaga–Luttinger-liquid state in carbon nanotubes at low temperatures. *Nature* **426,** 540–544 (2003).
21. Hillenbrand, R., Knoll, B. & Keilmann, F. Pure optical contrast in scattering-type scanning near-field microscopy. *J. Microsc.* **202,** 77–83 (2001).
22. Bechtel, H. A., Muller, E. A., Olmon, R. L., Martin, M. C. & Raschke, M. B. Ultrabroadband infrared nanospectroscopic imaging. *Proc. Natl Acad. Sci. USA* **111,** 7191–7196 (2014).
23. Gerber, J. A., Berweger, S., O'Callahan, B. T. & Raschke, M. B. Phase-resolved surface plasmon interferometry of graphene. *Phys. Rev. Lett.* **113,** 055502 (2014).
24. Boltasseva, A. & Atwater, H. A. Low-loss plasmonic metamaterials. *Science* **331,** 290–291 (2011).
25. Arnold, M. S., Green, A. A., Hulvat, J. F., Stupp, S. I. & Hersam, M. C. Sorting carbon nanotubes by electronic structure using density differentiation. *Nature Nanotech.* **1,** 60–65 (2006).
26. Fei, Z. *et al.* Gate-tuning of graphene plasmons revealed by infrared nano-imaging. *Nature* **487,** 82–85 (2012).
27. Chen, J. *et al.* Optical nano-imaging of gate-tunable graphene plasmons. *Nature* **487,** 77–81 (2012).
28. Liu, K. H. *et al.* High-throughput optical imaging and spectroscopy of individual carbon nanotubes in devices. *Nature Nanotech.* **8,** 917–922 (2013).
29. Palik, E. D. *Handbook of Optical Constants of Solids* (Elsevier, 1997).
30. Suzuura, H. & Ando, T. Phonons and electron–phonon scattering in carbon nanotubes. *Phys. Rev. B* **65,** 235412 (2002).

Acknowledgements

The authors thank M. Raschke for discussions. H.B. and M.M., in particular, thank M. Raschke and his group for the years of pioneering research on infrared near-field techniques and key collaborations that led to the development of a near-field infrared instrument at the Advanced Light Source (ALS). The authors also thank K. Liu, Y. Sun, S. Shi, C. Jin and H. Chang for their help with sample preparation and discussions. This work was primarily supported by the Office of Basic Energy Science, Department of Energy (contract no. DE-AC02-05CH11231, Sub-Wavelength Metamaterial Program; contract no. DE-SC0003949, Early Career Award). Spectroscopy of nanotubes in the visible range was supported by the National Science Foundation (grant no. DMR-1404865). The ALS is supported by the Director, Office of Science, Office of Basic Energy Sciences, of the US Department of Energy (contract no. DE-AC02-05CH11231). F.W. acknowledges support from a David and Lucile Packard fellowship.

Author contributions

F.W. and Z.S. conceived the project. Z.S. and X.H. prepared the nanotube samples. Z.S., H.B. and M.C.M. performed the near-field infrared measurements. X.H. and Z.B. performed visible spectroscopy. K.W. and T.T. provided the hBN crystals. X.H., Z.S., Y.R.S. and F.W. analysed the data. All authors discussed the results and contributed to writing the manuscript.

Additional information

Supplementary information is available in the online version of the paper. Reprints and permissions information is available online at www.nature.com/reprints. Correspondence and requests for materials should be addressed to Z.S. and F.W.

Competing financial interests

The authors declare no competing financial interests.